Radial profiles of temperature and viscosity in the Earth's mantle inferred from the geoid and lateral seismic structure

O. Čadek [a,*], A.P. van den Berg [b]

[a] Department of Geophysics, Faculty of Mathematics and Physics, Charles University, V Holešovičkách 2, 18000 Prague, Czech Republic
[b] Department of Theoretical Geophysics, University of Utrecht, Budapestlaan 4, 3805 TA Utrecht, Netherlands

Abstract

In the framework of dynamical modelling of the geoid, we have estimated basic features of the radial profile of temperature in the mantle. The applied parameterization of the geotherm directly characterizes thermal boundary layers and values of the thermal gradient in the upper and lower mantle. In the inverse modelling scheme these parameters are related to the observables (geoid and seismic structure of the mantle) through the viscosity profile which is parameterized as an exponential function of pressure and temperature. We have tested $\sim 10^4$ model geotherms. For each of them we have found proper rheological parameters by fitting the geoid with the aid of a genetic algorithm. The geotherms which best fit the geoid show a significant increase of temperature ($\sim$600–800ºC) close to the 660-km discontinuity. The value of the thermal gradient in the mid-mantle is found to be sub-adiabatic. Both a narrow thermal core–mantle boundary layer and a broad region with a superadiabatic regime can produce a satisfactory fit of the geoid. The corresponding viscosity profiles show similarities to previously presented models, in particular in the viscosity maximum occurring in the deep lower mantle. The best-fitting model predicts the values of activation volume V^* and energy E^* which are in a good agreement with the data from mineral physics, except for V^* in the lower mantle which is found somewhat lower than the estimate based on melting temperature analysis. An interesting feature of the viscosity profiles is a local decrease of viscosity somewhere between 500 and 1000 km depth which results from the steep increase of temperature in the vicinity of the 660-km discontinuity. © 1998 Elsevier Science B.V. All rights reserved.

Keywords: geoid; mantle; thermodynamic properties; geothermal gradient; viscosity

1. Introduction

The present-day estimates of mantle viscosity are based on microphysical investigation of creep mechanisms in polycrystalline silicates and oxides, and on analysis of the geophysical data related to the Earth's response to surface and internal loading [1]. These two approaches have so far been applied rather independently. The geophysical observables, namely the geoid and the post-glacial rebound data, have been used to constrain the viscosity models parameterized in term of layers of constant viscosity (for a review see, e.g., [2–4]). Attempts to include physical information about the temperature and pressure effects into this approach have so far been rare [5]. The main obstacle in the application of the microphysical models is their dependence on the deformation history,

* Corresponding author. Tel.: +42 2 8576 2544; Fax: +42 2 8576 2555; E-mail: peter@hervam.troja.mff.cuni.cz

composition and state conditions of the mantle which are broadly unknown [1,6]. The radial profile of temperature still belongs among the least known mantle parameters [7,8]. This, together with other uncertainties (grain size, effect of volatiles, etc.), makes any geophysical application of the microphysical models rather problematic.

In the present paper we include the basic information about mantle rheology from microphysics into the framework of dynamical modelling of the geoid. Assuming that the viscosity increases exponentially with pressure and decreases with temperature, and applying the standard technique for evaluating the response of a viscous body to lateral density differences [9], we will estimate such characteristics of mantle geotherms that are compatible with the observed long-wavelength geoid. A viscosity model which forms a link between the data and the temperature profile will be an important by-product of our inversion.

2. Parameterization

We use an exponential function of temperature and pressure for the viscosity model which represents a smooth approximation of the full Arrhenius form in terms of activation energy and volume [10]. As a first approximation we can write:

$$\eta_{um} = a_1 \exp[b_1 z - c_1 T(z)] \tag{1}$$

$$\eta_{lm} = a_2 \exp[b_2 z - c_2 T(z)] \tag{2}$$

where η_{um} and η_{lm} denote the viscosity of the upper and lower mantle respectively, z is the depth, T is the temperature, and a_i, b_i and c_i, $i = 1, 2$, are positive functions which, in general, vary with spatial variables. For simplicity, we will assume that a_i, b_i and c_i are constant parameters. Since the amplitudes of the long-wavelength geoid do not depend on the absolute value of viscosity but only on its relative changes [9], we can put $a_1 = 1$. The viscosity model of the mantle is then characterized by five constants (a_2, b_1, b_2, c_1 and c_2), and a radial profile of temperature $T(z)$.

The parameterization of the mantle geotherm $T(z)$ employed in this study is shown in Fig. 1. The geotherm is defined by eight parameters. Four

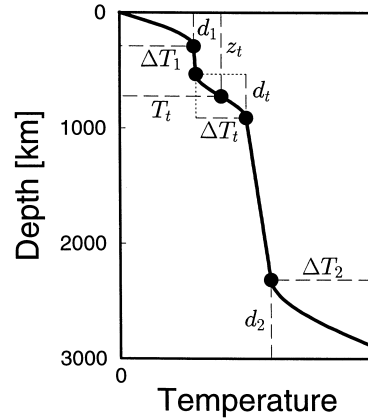## Parameterization of the geotherm

Fig. 1. Parameterization of the geotherm used in this paper.

parameters, d_1, d_2, ΔT_1 and ΔT_2 characterize the top and bottom boundary layer, and another four parameters, d_t, T_t, ΔT_t and z_t are used to describe the increase of temperature across the boundary between the upper and lower mantle. The temperature curve in the boundary layers is modelled by a simple harmonic function. Between the boundary layers the temperature increases linearly. We assume that the value of z_t is close to 660 km (600 km $< z_t <$ 800 km) and the thickness d_t of the thermal transition zone does not exceed 500 km. The temperature at the core–mantle boundary is normalized to 1.

The total number of parameters needed to describe the viscosity model is 13. This number is comparable to the number of layers used in recent inferences of viscosity from the long-wavelength geoid (e.g. [11–13]). In comparison with the layered models, the parameterization described above has a number of advantages. First of all, the viscosity in our model has to follow the basic physical trends which are imposed by a monotonous increase of pressure with depth and by the existence of the top and bottom thermal boundary layers. Except for the interface at a depth of 660 km, the viscosity defined by Eqs. 1 and 2 is a smooth, non-oscillating function of the depth. The parameterization does not require any additional choice of viscosity interfaces and, consequently, there is no trade off between the viscosity in the layer and the layer thickness which generally affects the layered viscosity models. The main

limitation of our parameterization is the assumption that the parameters a_i, b_i and c_i do not change with depth. Although the depth changes of these parameters can easily be included into the inversion scheme (see below), it is obvious that further increase of the number of formal free parameters would lead to a strong non-uniqueness of the solution due to a limited resolution power of the geoid [3,12].

3. Inversion

The lateral changes of density in the mantle, mapped by seismic tomography, induce the flow which deforms the surface and internal density interfaces. The gravity signal generated by topographies of these interfaces contributes to the observed geoid and its sign and magnitude strongly depend on the viscosity structure [9]. The attempts to infer the radial profile of viscosity from the geoid date back to the mid-eighties [3,5,11–18]. In this paper we follow the traditional inversion scheme described, e.g., by King [12] to determine the viscosity profile parameterized as described above. We minimize the squared misfit between the observed and predicted non-hydrostatic geoid. Only radial changes of viscosity are investigated. The effects of lateral variations in viscosity and compressibility are not considered. The surface of the Earth as well as the core–mantle interface are modelled as free-slip boundaries [3]. No boundary condition is imposed at the 660-km discontinuity. The problem is solved in the spectral domain [9].

The lateral distribution of density anomalies in the mantle is computed from the tomographic model by Su et al. [19] which is scaled by a constant factor $\partial \ln \rho / \partial \ln v = 0.25$. This value roughly corresponds to the velocity-to-density scaling given for S-wave by Karato [20]. Both the tomographic model and the geoid data are employed at harmonic degrees 2–12.

The inverse scheme consists of two steps. In the first step we have used around 10^4 randomly generated geotherm parameterized as in Fig. 1. In the second step, the rheological parameters a_2, b_1, b_2, c_1 and c_2, see Eqs. 1 and 2, have been determined for each of the geotherms by a genetic algorithm [12,21]. This strategy has allowed us to select a group of mantle geotherms which produce a reasonable ($\sim 70\%$) re-

duction of the misfit and, thus, can be regarded as compatible with the long-wavelength geoid.

4. Temperature profiles

Recent application of the global inverse techniques [12,13,18] has revealed a strongly non-unique nature of the geoid inversion. This conclusion is fully confirmed by the results of our study: among 10^4 randomly chosen geotherms we have been able to find around 20 profiles which give the reduction of the geoid misfit better than 70%. Four typical profiles are shown in Fig. 2. A comparison of the profiles in this figure gives an approximate idea about the uncertainties of the solution. The characteristics of the profiles are given in Table 1 (top).

The 70% variance reduction is found if the temperature in the lower mantle is significantly higher than in the upper mantle. The best fit to the geoid is obtained for a steep increase of temperature at least by $\Delta T_t = 0.2 T_{cmb}$ somewhere in the depth interval of 500–1000 km. This feature is rather robust as it is evident from Fig. 3, where the maximum variance reduction is plotted as a function of ΔT_t. The exact thickness and position of the upper/lower mantle thermal boundary layer is not well resolved by the data (see Fig. 2). Both a narrow thermal boundary layer located above the 660-km discontinuity (model
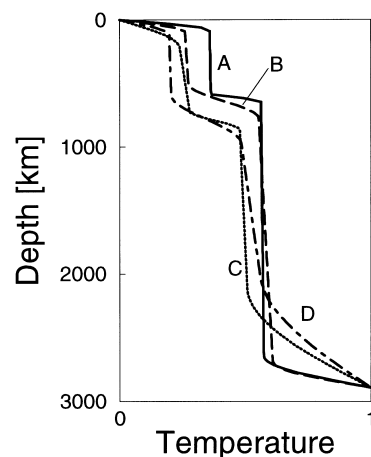

Fig. 2. Four model geotherms reducing the misfit by 70%. The differences between the models illustrate uncertainties of the solution.

Table 1
Basic characteristics of the geotherms giving a 70% reduction of the geoid misfit function

Parameter	A priori limit	Models with 70% variance reduction
d_1	80–300 km	80–300 km
ΔT_1	0.20–0.50 T_{cmb}	0.20–0.37 T_{cmb}
T_t	0.25–0.55 T_{cmb}	0.30–0.47 T_{cmb}
d_t	0–500 km	0–360 km
ΔT_t	0.00–0.30 T_{cmb}	0.2–0.3 T_{cmb}
d_2	100–1000 km	200–900 km
ΔT_2	0.20–0.60 T_{cmb}	0.38–0.50 T_{cmb}
β_1	0.0–0.6 T_{cmb}/z_{cmb}	0–0.45 T_{cmb}/z_{cmb}
β_2	0.0–0.6 T_{cmb}/z_{cmb}	0–0.22 T_{cmb}/z_{cmb}

β_1, β_2 — values of thermal gradient in the upper resp. lower mantle; T_{cmb} — temperature at depth $z_{cmb} = 2890$ km.

A in Fig. 2) and a broad thermal transition zone in the top part of the lower mantle (model D) can well account for the non-hydrostatic geoid.

The best-fitting geotherms are characterized by low, sub-adiabatic values of the thermal gradient in the lower mantle. According to our temperature models, the value of the thermal gradient in the mid-mantle should not exceed 0.3°C/km provided that $T_{cmb} < 4000$°C.

Another well resolved parameter is the temperature increase ΔT_2 in the bottom boundary layer, the value of which ranges between 0.4 and 0.5 T_{cmb}. In contrast, the thickness of the bottom boundary layer remains rather uncertain: Both a very narrow (~100 km) boundary layer and a broad (~800 km)
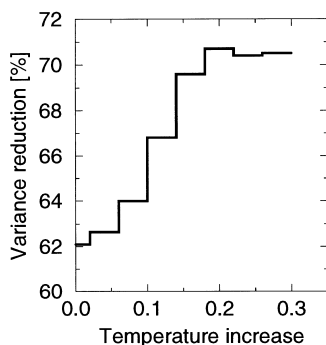
superadiabatic zone are found to be compatible with the geoid and available seismic tomographic information. A narrow boundary layer is predicted in traditional numerical simulations of mantle convection without pressure dependent viscosity. Possible existence of a broad superadiabatic region in the bottom half of the lower mantle has been recently discussed from the microphysical point of view [8]. The broad superadiabatic zone together with an overlying subadiabatic region has also been found in numerical modelling results based on pressure dependent viscosity [22].

5. Viscosity profiles

Fig. 4 shows the viscosity profiles corresponding to the model geotherms plotted in Fig. 2. Only the relative changes of viscosity can be inferred from this figure since the geoid is insensitive to the absolute value of viscosity [9]. All the models are normalized so that the viscosity at the surface is equal to 1. In general, the resultant viscosity models can be classified into two groups.

The first group, represented by models A and B, corresponds to the geotherms with the mid-mantle temperature increase located mostly above the 660

Fig. 3. The maximum reduction of the geoid misfit as a function of ΔT_t (see Fig. 1). The graph was constructed from the results obtained for 10^4 randomly chosen temperature profiles, which were classified into 7 intervals according to the value of ΔT_t.
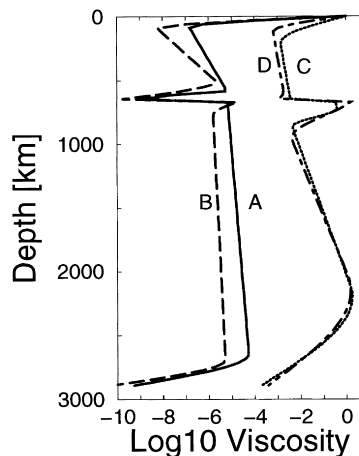
Fig. 4. Four models of viscosity corresponding to the temperature profiles in Fig. 2. Each of the models reduces the geoid misfit at least by 70%. The models are normalized so that the viscosity on the top of the lithosphere is 1. Only the relative changes of viscosity can be inferred from this figure.

km discontinuity. The viscosity models of this group are characterized by a stiff lithosphere, a deep asthenosphere between 100 and 400 km depth and a viscosity peak around a depth of 500 km. Below the 660-km boundary, the viscosity only weakly increases peaking at a depth of about 2700 km. In the core–mantle boundary layer the value of viscosity drops by several orders. The most remarkable feature of these viscosity models is a narrow low-viscosity zone located above the 660-km discontinuity. The existence of such a zone was first discussed by Forte and co-workers [16]. Possible decrease of viscosity in the transition zone or somewhat deeper, at a depth between 660 and 1000 km, was independently reported by other authors, mostly as a result of the geoid inversions [12,14,18,23] or the numerical simulations of thermal convection with an endothermic phase transition (e.g. [24]). From the mineralogical point of view, the decrease of viscosity below the 660-km discontinuity would be a natural consequence of the increase of temperature due to a limited convective heat transfer in this region [1,6].

The other group of models (models C and D in Fig. 4) is derived from the temperature profiles which show a significant increase of temperature in the top part of the lower mantle. The lithosphere of these models is weaker than in the models of the first group and the asthenosphere is not clearly defined. The viscosity of the sub-lithospheric upper mantle is almost constant. Around a depth of 660 km the viscosity steeply increases by 2–3 orders of magnitude, peaking somewhere between 660 and 800 km. Below this depth the viscosity forms a broad low viscosity zone. In the real mantle, the existence of such a zone would probably lead to a reduction of the mass exchange across the 660-km discontinuity [25]. The minimum value of viscosity is usually reached somewhere between 800 and 1000 km depth. Below a depth of 1000 km the viscosity again increases forming a broad viscosity maximum at a depth between 2000 and 2500 km. Except for the viscosity peak around a depth of 660 km, the profiles are almost identical with the viscosity model derived from the geoid by Ricard and Bai [11].

The existence of two different groups of viscosity models, predicting the same portion of the geoid, confirms the non-unique nature of the geoid inversion, first discussed by King [12] and recently

Table 2
Estimates of the rheological parameters

Model	A	B	C	D
a_2/a_1	8.4	18.4	15.1	25.6
b_1^a	48.4	22.5	13.2	7.8
b_2 [a]	4.3	3.4	15.1	22.0
c_1 [a]	78.4	45.5	31.3	38.3
c_2 [a]	30.0	27.7	26.4	33.1
V_1^* (cm^3/mol)	5.0	1.8	0.9	0.5
V_2^* (cm^3/mol)	0.7	0.5	2.2	2.9
E_1^* (kJ/mol)	370	110	70	50
E_2^* (kJ/mol)	340	310	220	280

[a] Value for z and T, Eqs. 1 and 2, normalized to 1.

corroborated by Pari and Peltier [26]. A thorough discussion of different viscosity profiles from the viewpoint of mineral physics can be found in [1,6] where similar viscosity models as presented in this paper are proposed.

An inspection of Eqs. 1 and 2 suggests that there is a trade-off between the rheological parameters a_i, b_i and c_i on the one hand and the parameters characterizing the geotherm $T(z)$ on the other. The dispersion of the values of model parameters a_i, b_i and c_i, that give a satisfactory fit of the geoid, has been found indeed large although certain bounds can be estimated (see Table 2, top part). The temperature dependence of the viscosity is generally smaller in the lower mantle compared to the upper mantle ($c_2/c_1 < 1$). The results for the pressure dependence are ambiguous. The pressure dependence of the upper mantle viscosity is found to exceed the value for the lower mantle ($b_2/b_1 < 1$) in the case of geotherms A and B, while the opposite result ($b_2/b_1 > 1$) is found for profiles C and D. The latter type of viscosity models, characterized by a strong pressure dependence of viscosity in the lower mantle, would result in a stiff deep-lower mantle with strongly reduced convective heat transport [22] which is consistent with a broad superadiabatic layer found in geotherms C and D (Fig. 2).

6. Comparison with laboratory data

In the bottom part of Table 2, we give the values of activation volume V^* and activation energy E^* es-

timated from parameters b and c through equations:

$$V^* = \frac{bR\langle T\rangle}{\rho g},$$ (3)

$$E^* = \frac{c}{R\langle T\rangle^2}$$ (4)

where R is the gas constant, $\langle T\rangle$ the average temperature, ρ the density, and g the gravity acceleration. The values of E^* and V^* listed in Table 2 have been computed from appropriate parameters b and c for $T_{cmb} = 4000$ K, $g = 10$ ms^{-2} and $\rho = 4500$ kg m^{-3}. These values can directly be compared with the estimates from mineral physics [1,8,27–29]. The laboratory data on olivine suggest that the value of V^* in the upper is ~5 cm^3 mol^{-1} for diffusion creep and ~15 cm^3 mol^{-1} for dislocation creep [29]. At present, there are no data on V^* for the lower mantle. A rough estimate of V^* can be obtained from melting data by using the Weertman scaling with homologous temperature [8]. Employing the recent data on melting temperature by Zerr and co-workers [30] and estimate of E^* by Yamazaki et al. [28], one would expect $V^* \sim 4$–10 cm^3 mol^{-1}. The value of activation energy E^* estimated for olivine from laboratory experiments ranges between 240 and 300 kJ mol^{-1} for diffusion creep, and between 430 and 540 kJ mol^{-1} for dislocation creep [27]. In the lower mantle, E^* is expected to be ~300–340 kJ mol^{-1} [28].

A remarkable agreement with the above parameters, found for the diffusion creep in olivine under the upper mantle conditions, have been obtained for model A. It should be noted that this model also gives the best fit to the observed geoid among all the tested models. In the lower mantle, model A perfectly predicts the laboratory estimate of E^* but gives too small value of V^*. If we admit that the value of $V^* \sim 1$ found in our inversion for model A is roughly correct, the melting temperature in most of the lower mantle has to be below 2000 K which is significantly less than recently estimated by Zerr and co-workers [30]. The values of activation parameters found for model B are similar as for model A in the lower mantle and about three times smaller in the upper mantle. The other group of models, represented by profiles C and D, gives rather small values of activation parameters in the upper mantle. In the lower mantle, the value of V^* approaches the lower

bound of admissible values discussed above, and the value of E^* is found close to the laboratory estimate of Yamazaki et al. [28].

Under the present stage of knowledge in mineral physics, it is rather difficult to discriminate between the two groups of models presented in this paper. The very good fit to the observed geoid and the agreement with the laboratory data in the upper mantle favor model A, characterized by two low viscosity zones in the upper mantle and relatively small changes in viscosity with depth (with exception of the boundary layers). This model fits quite well the available mineral physics information except for V^* in the lower mantle. It is also likely that models A and B would better fit the observation of postglacial rebound and sea-level changes than models of the other groups (C and D) which show a large increase of viscosity in the deep lower mantle. On the other hand, models C and D, which give unrealistic values of activation parameters in the upper mantle, are in a good agreement with the hypothetical existence of a broad superadiabatic zone in the lowermost mantle, recently supported by microphysical investigation [8] and numerical simulations of mantle convection [22], and predict reasonable values of V^* and E^* in the lower mantle. The above discussion suggests that further mineral physics constraints and laboratory data, especially for the lower mantle, could significantly help to eliminate the non-uniqueness of the geoid modelling.

7. Limitations of inversion

Similarly to other dynamical models based on modelling the dynamical geoid, the results presented here suffer from a number of limitations due to the physical and formal simplifications. Certain caution is thus necessary in interpreting the models and their further applications in mineral physics and geodynamics. The uncertainties of the models presented here can be classified into four groups.

(1) *Uncertainties in tomographic models.* In this paper we present the results obtained for an S-wave tomographic model derived by the Harvard group [19]. Although the basic features of this model are in agreement with other tomographic models, certain differences between various tomographic models, in

particular between S- and P-wave models, still remain and they may be of physical or compositional origin [31]. Preliminary tests carried out for other S-wave tomographic models [32,33] suggest, however, that the results of the inversion do not depend much on which tomographic model is employed.

(2) *Translation of seismic anomalies to densities*. We have assumed that the density anomalies generating the flow in the mantle are proportional to the seismic anomalies imaged by seismic tomography. This may not be correct in a large portion of the upper mantle where the seismic anomaly pattern is probably strongly influenced by petrological heterogeneities [34]. The role of petrological changes in the lower mantle may also be important, especially close to the core–mantle boundary [35,36]. Even if the role of thermal anomalies is dominant in the whole mantle and, thus, $\delta\rho \sim \delta v$ as assumed in this paper, the velocity-to-density scaling factor $(\partial \ln \rho / \partial \ln v)$ will probably vary with depth, in contrast to the present paper in which a constant value of $(\partial \ln \rho / \partial \ln v)$ is assumed. As already mentioned above, further increase of the number of free parameters would lead to a strong non-uniqueness of the inverse problem and, thus, a radially dependent $(\partial \ln \rho / \partial \ln v)$ can hardly be included in the set of unknowns. On the other hand, several studies have demonstrated that weak changes of $(\partial \ln \rho / \partial \ln v)$ with depth, which may be indeed the case of the real mantle [20], do not much influence the resultant viscosity profiles [12,18].

(3) *Boundary conditions at the top boundary and at the interface between upper and lower mantle*. We have assumed that the physical conditions at the surface can be approximated by free slip and we have neglected the surface forces which may result from the mineral changes at the boundary between the upper and lower mantle. Čadek and Fleitout [37] have recently demonstrated that the free slip may not be appropriate for the top mantle boundary and that the non-uniqueness of the inversion can be significantly reduced if the observed plate velocities are imposed at the base of the lithosphere. The long-wavelength forces acting at the 660-km discontinuity and hampering the mass exchange between the upper and lower mantle have been discussed by several authors [38,39]. It is obvious that further studies of this type will have to link the increase in temperature at

the upper/lower mantle interface with a force which restrains the vertical flux across the boundary.

(4) *Simplifications in rheology*. We have assumed a temperature dependent viscosity (Eqs. 1 and 2) but we have neglected the variations in viscosity associated with lateral changes of temperature. This apparent inconsistency has been justified by relatively small effects of the lateral variations in viscosity on the prediction of the dynamical geoid [23]. Only a linear (Newtonian) approximation has been considered here. This is motivated both by practical considerations because of the large computational costs of a non-Newtonian rheology [23,40] and by evidence for predominantly Newtonian flow in large parts of the mantle [41].

The above drawbacks and pitfalls are common to most of the published models of the dynamical geoid. The agreement with the mineral physics data reached here, however, indicates that the effects of the above simplifications may not be too important and some features of the derived models, namely the thermal increase at a depth of about 660 km, may be robust.

8. Concluding remarks

The success of any inversion of the geophysical data depends on a suitable choice of the model parameters. In this paper, the geoid is used to constrain the depth changes of viscosity which is parameterized in terms of temperature and pressure. A comparison of the resultant temperature and viscosity profiles (Figs. 2 and 4) indicates that the results obtained for temperature show smaller dispersion than the viscosity models. This suggests that the temperature, which is directly linked to the energy driving the flow in the mantle, may be a suitable quantity for this type of inverse modelling. The microphysical analysis together with the mineral physics experiments and the results of numerical simulations of thermal convection may provide further constraints which can be used to eliminate the non-uniqueness of the inversion. The preliminary results presented here can be understood as an attempt to contribute to the formation of a general model of the Earth which would be consistent with the thermal processes governing its evolution (cf. [26,42]).

Acknowledgements

References

[1] G. Ranalli, Inferences on mantle rheology from creep laws, in: P. Wu (Ed.), Dynamics of the Ice Age Earth, A Modern Perspective, Trans Tech Publications, 1998, pp. 323–340.

[2] K. Lambeck, P. Johnston, C. Smither, M. Nakada, Glacial rebound of the British isles — III. Constraints on mantle viscosity, Geophys. J. Int. 125 (1996) 340–354.

[3] C. Thoraval, M.A. Richards, The geoid constraint in global geodynamics: viscosity structure, mantle heterogeneity models and boundary conditions, Geophys. J. Int. 131 (1997) 1–8.

[4] J.X. Mitrovica, A.M. Forte, Radial profile of mantle viscosity: Results from the joint inversion of convection and postglacial rebound observables, J. Geophys. Res. 102 (1997) 2751–2769.

[5] V. Corrieu, Y. Ricard, C. Froidevaux, Converting mantle tomography into mass anomalies to predict the Earth's radial viscosity, Phys. Earth. Planet Inter. 84 (1994) 3–13.

[6] S. Karato, Phase transformations and rheological properties of mantle materials, in: D. Crossley, A.M. Soward (Eds.), Earth's Deep Interior, chapter 8, Gordon-Breach, 1996.

[7] R. Boehler, Temperature in the Earth's core from melting-point measurements of iron at high static pressure, Nature 363 (1993) 534–536.

[8] S. Karato, Effects of pressure on plastic deformation of polycrystalline solids: Some geological applications, in: R.M. Wentzcovitch et al. (Eds.), High Pressure Research in Material Science, Material Research Society, Pittsburgh, PA, in press, 1998.

[9] B.H. Hager, R.W. Clayton, Constraints on the structure of mantle convection using seismic observations, flow models and the geoid, in: W.R. Peltier (Ed.), Mantle Convection, Plate Tectonics and Global Dynamics, Gordon Breach, 1989, pp. 657–763.

[10] U.R. Christensen, Convection with pressure- and temperature-dependent non-Newtonian rheology, Geophys. J. R. Astron. Soc. 77 (1984) 343–384.

[11] Y. Ricard, Bai Wuming, Inferring the viscosity and the 3-D density structure of the mantle from geoid, topography and plate velocities, Geophys. J. Int. 105 (1991) 561–571.

[12] S.D. King, Radial models of mantle viscosity: Results from a genetic algorithm, Geophys. J. Int. 122 (1995) 725–734.

[13] O. Čadek, H. Čížková, D.A. Yuen, Can long-wavelength dynamical signature be compatible with layered mantle convection?, Geophys. Res. Lett. 24 (1997) 2091–2094.

[14] S.D. King, G. Masters, An inversion for radial viscosity structure using seismic tomography, Geophys. Res. Lett. 19 (1992) 1551–1554.

[15] J. Morgan, P.M. Shearer, Seismic constraints on mantle flow and topography of the 660-km discontinuity: Evidence for the whole-mantle convection, Nature 365 (1993) 506–511.

[16] A.M. Forte, A.M. Dziewonski, R.L. Woodward, Aspherical structure of the mantle, tectonic plate motions, nonhydrostatic geoid and topography of the core–mantle boundary, in: J.-L. Mouel (Ed.), Dynamics of the Earth's Deep Interior and Earth Rotation, Geophys. Monogr. Ser. 72 (1993) 135–166, AGU, Washington, DC.

[17] G. Pari, W.R. Peltier, The heat flow constraint on mantle tomography-based convection models: Towards a geodynamically self-consistent inference of mantle viscosity, J. Geophys. Res. 100 (1995) 12731–12752.

[18] M. Kido, O. Čadek, Inferences of viscosity from the oceanic geoid: Indication of a low viscosity zone below the 660-km discontinuity, Earth Planet Sci. Lett. 151 (1997) 125–138.

[19] W.-J. Su, R.L. Woodward, A.M. Dziewonski, Degree 12 model of shear velocity heterogeneity in the mantle, J. Geophys. Res. 99 (1994) 6945–6980.

[20] S. Karato, Importance of anelasticity in the interpretation of seismic tomography, Geophys. Res. Lett. 20 (1993) 1623–1626.

[21] D.E. Goldberg, Genetic Algorithms in Search, Optimization, and Machine Learning, Addison-Wesley, 1989.

[22] A.P. van den Berg, D.A. Yuen, Temperature at the core–mantle boundary (CMB) as a control variable in modelling planetary dynamics, Phys. Earth Planet. Inter. 108 (1998) 219–234.

[23] S.S. Zhang, U.R. Christensen, Some effects of lateral viscosity variations on geoid and surface velocities induced by density anomalies in the mantle, Geophys. J. Int. 114 (1993) 531–547.

[24] D. Brunet, Ph. Machetel, Mantle avalanche effect with temperature, pressure and phase dependent viscosity, J. Geophys. Res. 103 (1998) 4929–4945.

[25] L. Cserepes, D.A. Yuen, Dynamical consequences of mid-mantle viscosity stratification on mantle flows with the endothermic phase transition, Geophys. Res. Lett. 24 (1997) 181–184.

[26] G. Pari, W.R. Peltier, Global surface heat flux anomalies from seismic tomography-based models of mantle flow: Implications for mantle convection, J. Geophys. Res. (1998) in press.

[27] S. Karato, P. Wu, Rheology of the upper mantle: A synthesis, Science 260 (1993) 771–778.

[28] D. Yamazaki, T. Kato, H. Yurimoto, E. Ohtani, M. Tori-

umi, Silicon self-diffusion in MgSiO$_3$ perovskite, Science submitted, 1990.

[29] S. Karato, D.C. Rubie, Toward an experimental study of deep mantle rheology: A new multianvil sample assembly for deformation studies under high pressures and temperatures, J. Geophys. Res. 102 (1997) 20111–20122.

[30] A. Zerr, A. Diegeler, R. Boehler, Solidus of Earth's deep mantle, Science 281 (1998) 243–246.

[31] B.L.N. Kennett, S. Widiyantoro, R.D. van der Hilst, Joint seismic tomography for bulk sound and shear wave speed in the Earth's mantle, J. Geophys. Res. 103 (1998) 12469–12493.

[32] G. Masters, S. Johnson, G. Laske, H. Bolton, A shear-velocity model of the mantle, Philos. Trans. R. Soc. London A 354 (1996) 1385–1411.

[33] J.H. Woodhouse, J. Trampert, New geodynamical constraints from seismic tomography, Earth Planet. Sci. Lett. submitted.

[34] M.-P. Doin, L. Fleitout, D. McKenzie, Geoid anomalies and the structure of continental and oceanic lithospheres, J. Geophys. Res. 101 (1996) 16119–16135.

[35] M.E. Wysession, C.R. Bina, and E.A. Okal, Constraints on the temperature and composition of the base of the mantle, in: J.-L. Le Mouel et al. (Eds.), Dynamics of the Earth's Deep Interior and Earth Rotation, Geophys. Monogr. Ser. (1993) 181–190, AGU, Washington, DC.

[36] T. Lay, Q. Williams, E.J. Garnero, The core–mantle boundary layer and deep Earth dynamics, Nature 392 (1998) 461–468.

[37] O. Čadek, L. Fleitout, A global geoid model with imposed plate velocities and partial layering (abstract), in: G. Hulot et al. (Eds.), 6th Symposium of SEDI, Tours, France, 1998.

[38] Y. Le Stunff, Y. Ricard, Partial advection of equidensity surfaces: A solution for the dynamic topography problem?, J. Geophys. Res. 102 (1997) 24655–24667.

[39] U.R. Christensen, Dynamic phase boundary topography by latent heat effects, Earth Planet. Sci. Lett. 154 (1998) 295–306.

[40] O. Čadek, Y. Ricard, Z. Martinec, C. Matyska, Comparison between Newtonian and non-Newtonian flow driven by internal loads, Geophys. J. Int. 112 (1992) 103–114.

[41] S. Karato, S. Zhang, H.R. Wenk, Superplasticity in Earth's lower mantle: Evidence from seismic anisotropy and rock physics, Science 270 (1995) 458–461.

[42] H.-P. Bunge, M.A. Richards, C. Lithgow-Bertelloni, J.R. Baumgardner, S.P. Grant, B.A. Romanowicz, Time scales and heterogeneity structure in geodynamics earth models, Science (1998) in press.